INVESTIGATION OF THE WIND FORCES ON RECTANGULAR OVERHANG BUILDINGS USING URANS

非定常 RANS を用いた矩形のオーバーハングを有する建物に作用する風力の検討

R&D センター　ドアン　セイ　ロン　LONG DOAN SY
R&D センター　小島　千里　CHISATO KOJIMA
R&D センター　川島　学　MANABU KAWASHIMA

本論文では，数値流体力学（CFD）技術を用いて，建物表面のさまざまな位置に矩形ブロックを配置した建物（オーバーハング建物）に作用する風力について，シミュレーションを実施した。具体的には，オーバーハング位置をパラメータとした 14 種類の建物モデルを作成し，Unsteady Reynolds-Averaged Navier-Stokes（URANS）を用いて，各モデルに作用する風力を推定した。風方向の風力係数の値が角柱建物と比較して最も変化するオーバーハング位置は，風上壁面下部位置である。オーバーハングが存在する場合の風力係数の変化は，風の剥離位置と前方および後方淀み点の変化が寄与していると考えられる。

キーワード：数値流体力学，非定常 RANS，オーバーハング建物，風力係数

This research paper investigates the wind forces exerted on buildings with overhang features placed at various positions on their surfaces, utilizing computational fluid dynamics (CFD) techniques. The Unsteady Reynolds-Averaged Navier-Stokes (URANS) turbulence models are employed to simulate the airflow patterns. Fourteen distinct configurations of overhang buildings are generated by introducing the rectangular block at different locations on the faces of a square building. The most different value of the along-wind force coefficient between the overhang building and the principal building is when the overhang is at the bottom in the upwind direction. The alteration in wind force coefficient in the presence of an overhang could be contributed by the position of the flow separation and the change in the front and rear stagnation points.

Key Words: Computational fluid dynamics, URANS, Overhang building, Wind force coefficient.

1. INTRODUCTION

In contemporary building design, the demand for increased living space in residential high-rise buildings has become increasingly significant. With limited land availability for development in densely populated megacities, skyscrapers have gained popularity. A unique type of high-rise structure is the overhang building, which features a small rectangular cylinder attached to it. Generally, in building design, the overhang structure is conventionally situated at the lower portion of the building, thereby creating podium floors. Nevertheless, certain instances deviate from this norm and opt to enlarge the upper section of the building instead. This approach aims to improve the residential unit area ratio of the upper floors, resulting in an overall increase in the value of both the living space and the commercial feasibility. An example of this high-value tower-style condominium is the Sulatto V Tower, which was introduced by Sumitomo Mitsui Construction Co., Ltd. (SMCC) in 2020[1].

The irregular shape such as a large size of overhang shape was studied by Yoshida et al.[2]. Wind pressure measurement was conducted using pressure taps on a large overhang situated from the bottom to near the top of the front face of a building, referred to as a step on the wall surface. Based on the minimum pressure coefficient results, the formation of a 3D vortex between the building and the overhang is discussed.

However, limited research has been conducted on inverted skyscrapers, where the overhang is positioned near the top of the building. Furthermore, the wind effects of the positioning of the overhang structure on the primary building are yet to be determined.

Computational Fluid Dynamics (CFD) has gained extensive usage for quantifying wind loading on structures and facilitating a profound comprehension of flow characteristics. In CFD, the Reynolds-Averaged Navier-Stokes (RANS) method has been widely known for its time-saving capabilities compared to other turbulence models in CFD such as Direct Numerical Simulation or Large-Eddy Simulation. The Unsteady RANS (URANS) is recognized as a suitable approach for predicting periodic turbulent separated flows[3]. In building science, URANS is possible to replicate large-scale fluctuations observed in the vicinity of tall buildings[4]. Nevertheless, the specific nature of fluctuations generated by URANS remains uncertain and necessitates validation through wind tunnel tests in most cases.

The presence of overhangs changes the aerodynamic characteristics around the structure and adds complexity to the assessment of load distribution and structural stability. This study aimed to assess the impact of wind forces on a primary square building by simulating its attachment to a rectangular-shaped overhang at different positions using CFD. Fourteen scenarios are simulated, considering various positions of the overhang on the front, rear, and side faces of the structure. Wind force coefficients in along-wind and across-wind direction are calculated to evaluate the influence of the rectangular overhang on the wind effects experienced by the primary square building.

2. ANALYSIS METHOD

Flow characteristics are predicted in this study using the ANSYS Fluent 2022R1 commercial numerical program. The ANSYS Fluent software, known for its extensive capabilities in fluid dynamics analysis, enables comprehensive investigations into the flow characteristics of complex systems.

URANS method is used in this study. The computational method employed is the semi-implicit method for pressure-linked equations (SIMPLE), and the turbulence model is k-ω shear stress transport (SST). k-ω SST model is used because it can effectively replicate the unsteady turbulence behind the high-rise building[4]. Also, k-ω SST has less computational time compared to the k-ω Reynolds stress model[5].

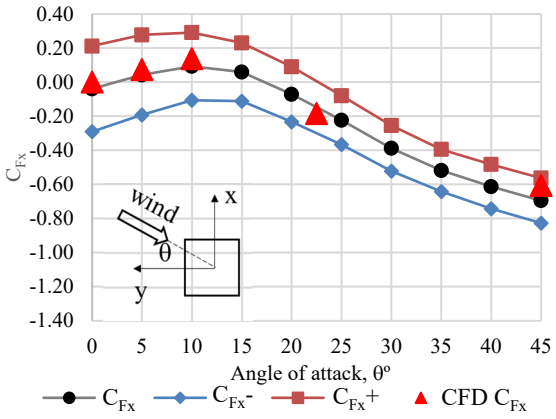

Fig. 1. Wind force coefficient in x-direction (C_{Fx})

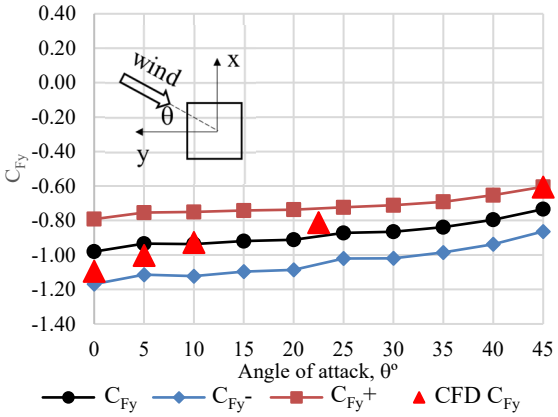

Fig. 2. Wind force coefficient in y-direction (C_{Fy})

$$C_F = \frac{F}{0.5\rho U_0^2 A} \quad (1)$$

The accuracy and reliability of URANS method were validated by comparing its results with wind tunnel experiments conducted at SMCC. The experiment used a square cylinder model with a height of 400mm and width of 58.8mm. The test covered angles from 0º to 45º in increments of 5º. Subsequently, the wind force coefficient C_F in each case was calculated using Equation (1), with F as the wind force on the x or y axis, ρ as the air density (1.225kg/m^3), U_0 as the reference wind velocity at the top of the building, and A as the area of the building face.

Fig. 1 and **Fig. 2** show a comparison between wind tunnel data and CFD calculations of wind force coefficients in the x- and y-directions at various angles of attack. The y-direction is the direction perpendicular to the building front face, and the angle of attack θ is the angle between the wind

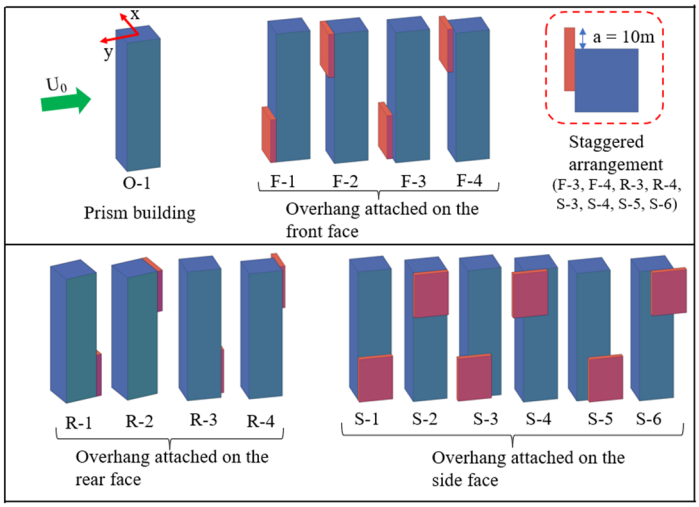

Fig. 3. Configuration cases

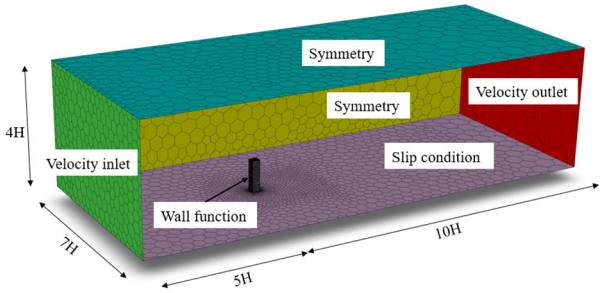

Fig. 4. CFD boundary conditions

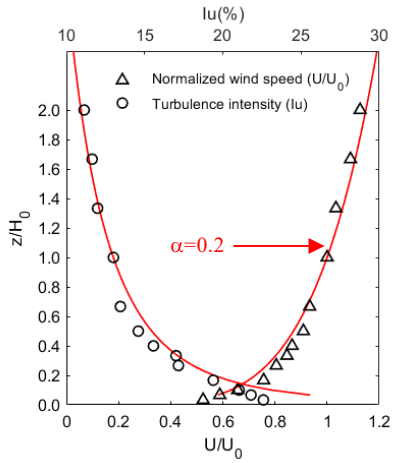

Fig. 5. Normalized wind velocity and turbulence intensity profiles

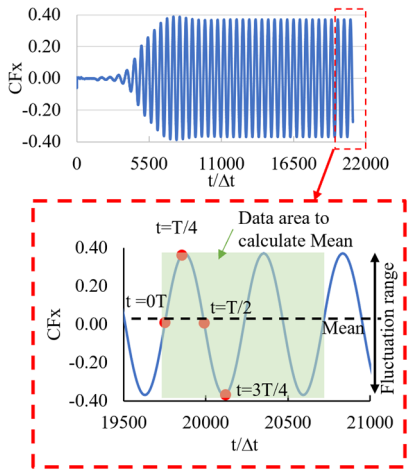

Fig. 6. Presented instantaneous points of across-wind force coefficient (C_{Fx}) at case O-1

direction and the y-direction. The symbols in the legend indicate mean (C_F), minimum (C_F-), and maximum (C_F+) coefficients in the x- and y-directions. The ▲ symbol is the result of the mean wind force coefficient C_F calculated by CFD. A comparison between the CFD calculation and the wind tunnel test results shows that the trend of the mean wind force coefficient with respect to the angle of attack is almost comparable.

3. ANALYSIS SETUP

The building model under analysis consists of a prototype square cylinder building with a height (H_0) of 120m and an aspect ratio of 4. Additionally, a rectangular overhang with dimensions of 30m×40m×5m (Width×Height×Depth) is introduced. To investigate the effect of the additional overhang on square cylinder in wind force at different positions on the principal building, the rectangular prism overhang is positioned in 14 different locations around the building's faces. Specifically, there are 4 cases on the front face, 4 cases on the rear face, and 6 cases on the side face, as

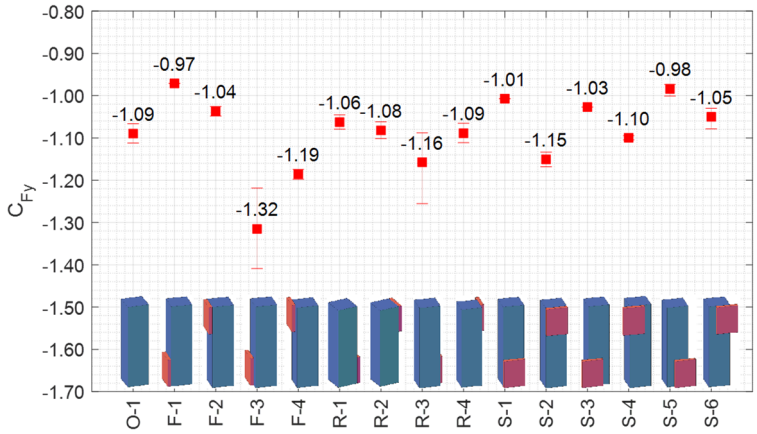

Fig. 7. Wind force coefficient in Y direction (C_{Fy})

visually represented in **Fig. 3**. In particular, the staggered arrangement cases, namely F-3, F-4, R-3, R-4, S-3, S-4, S-5, and S-6, are configured with an inclination of a = 10m.

The simulation domain is illustrated in **Fig. 4** with H is the model height. The simulation model is established at a scale of 1/400. **Fig. 5** presents the normalized wind velocity and turbulence intensity used as input flow. These parameters are combined with the wind profile recommended by the Architectural Institute of Japan (AIJ) in category of surface roughness III (power law component $\alpha = 0.2$) specifically for urban areas. The wind velocity at the top height of the model corresponds to U_0 = 8.92m/s. The Reynolds number considering the width of the model is 4.26×10^4.

An unstructured polyhedral mesh was used, with two refined areas for improved accuracy in critical regions. To accurately predict flow near wall using the wall function, Y+ value, which serves as a non-dimensional measure indicating the coarseness or fineness of a volumetric mesh in relation to a flow pattern, is put into consideration. For more accurate predictions or when using advanced turbulence models, Y+ values in the range of 1 to 5 are often preferred[6], and 5 is maintained to adequately capture the dynamics of flow near solid surfaces.

The CFD simulation conducted in this study terminates when the forces exerted on the structure reach a state of stability in unsteady flow conditions. In the subsequent section, instantaneous data points at four different time instances within one period (t=0T, T/4, T/2, 3T/4), as well as their corresponding mean values of two periodic periods, are presented as illustrated in **Fig. 6**. In this figure, the variation or change in the wind force coefficient over time when reaching the state of stability in unsteady flow conditions is called fluctuation range.

4. RESULTS AND DISCUSSION

4.1 EFFECT OF OVERHANG ON ALONG-WIND FORCE

Fig. 7 graphically illustrates the wind force coefficient in the y- direction, denoted as C_{Fy}. The calculation of the wind force coefficient is the same as section 2 with A is the area of the front face of the principal building and the same for all configuration cases. The fluctuation range of wind force coefficient in each case is also presented. Two main results can be observed from this figure. Firstly, large variations of the mean C_{Fy} are observed in group F compared to the principal building. The effect of the rectangular prism overhang on the mean C_{Fy} shows a range of variability, with up to a 10% decrease or 20% increase compared to the principal building, depending on the specific locations where the overhang is attached. On the other hand, the variations of mean C_{Fy} compared to principal building are relatively small in group R. Secondly, comparison of the lower and upper configuration of overhang on the same face in group F and R (F-1 to F-2; F-3 to F-4; R-1 to R-2 and R-3 to R-4), the absolute difference value of C_{Fy} between lower overhang buildings and the principal building (O-1) tend to be greater than the same difference in upper configuration.

The discussion on the variation of mean C_{Fy} in group F is based on the trend exhibited in the F and R groups. Also, the wind pressure coefficient distribution on the building's rear surface is presented in **Fig. 8**. F-1 and F-3, R-1 and R-2 are considered as examples. The pressure coefficient is calculated by $c_p = (p_t - p_\infty)/q_\infty$, where p_t is the total pressure, and p_∞ and q_∞ are the reference static pressure and dynamic pressures at the model height respectively. In F-1, the absolute value of negative pressure at the rear is observed

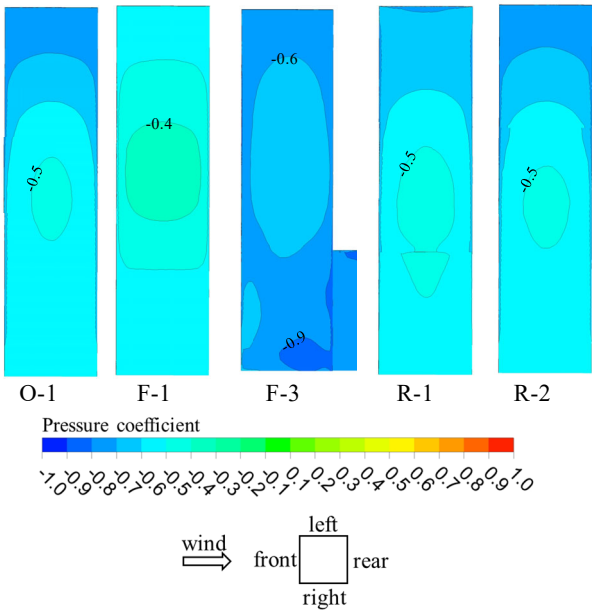

Fig. 8. Mean pressure coefficient distribution on the rear faces

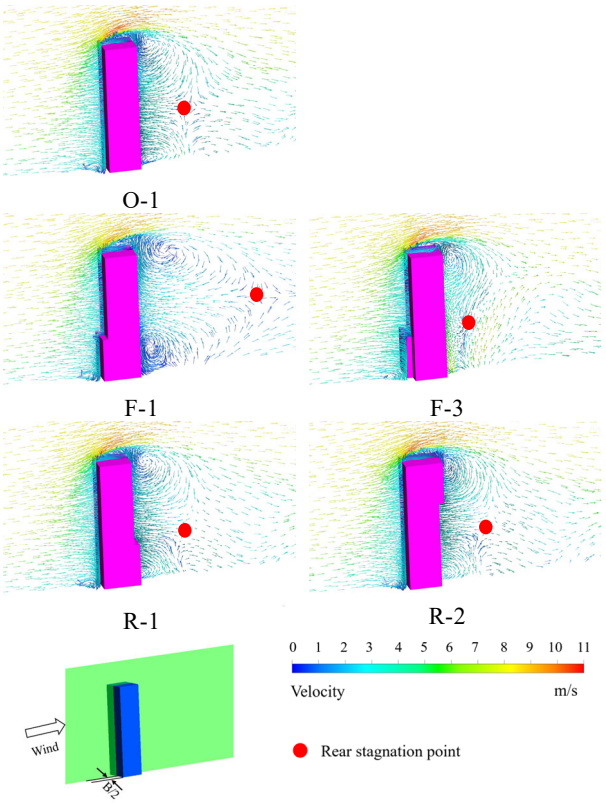

Fig. 9. Velocity contours at t=0T in the middle plan x = 0 and illustration of rear stagnation points

to be smaller in comparison to O-1, as shown in **Fig. 8**. A very high absolute value of negative pressure is experienced on the rear face of F-3. On the other hand, the pressures on the rear face in R-1 and R-2 are almost the same as in the principal building. **Fig. 9** presents the velocity vector figures

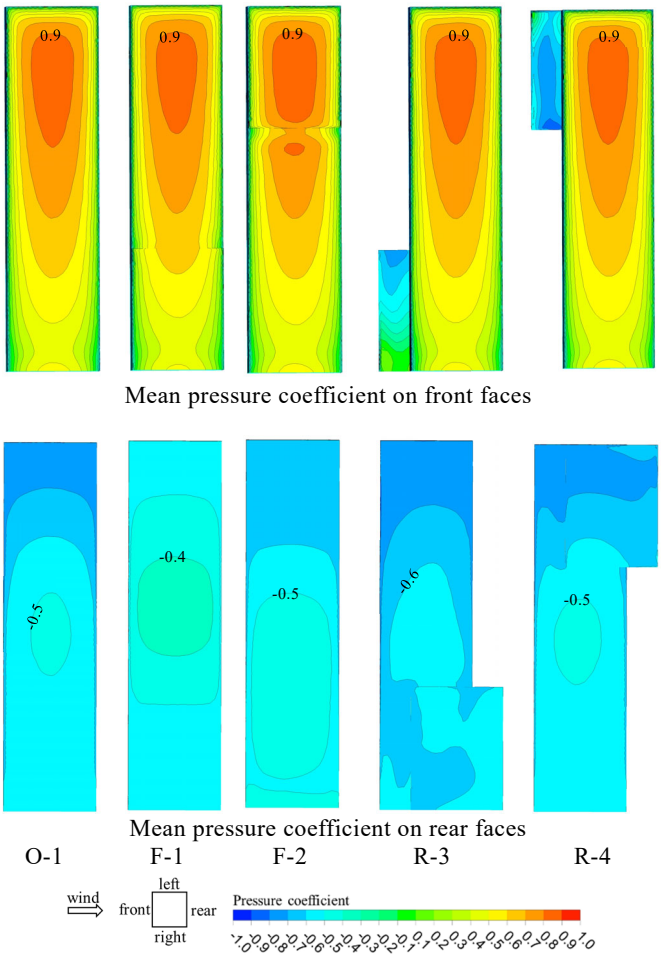

Fig. 10. Mean pressure coefficient distribution in case O-1; F-1; F-2; R-3 and R-4

at t=0T in the middle plans x = 0, and also illustrates the rear stagnation points in the principal building and some buildings in F and R group which are discussed above. The drag force tends to be higher when the rear stagnation point is closer to the rear surface in the downstream direction[7]. The rear stagnation points for F-1 and F-3 are significantly different from O-1. In these cases, the difference could come from the variation in how the flow separates around the overhang and the building's edge both at the top and bottom. In F-3, the wider front side of the building created by the overhang contributes to the formation of the vortex of separation flow at the corner on the side in the upwind direction. Consequently, the negative pressure at the back is higher compared to O-1 because of the suction effect created by this separation vortex caused by the overhang. On the other hand, in R-1 and R-2, the distance between the rear stagnation point and the rear of the building is almost the same as in the principal building. Due to this similarity, the rear negative pressure distribution is almost comparable in R-1, R-2, and

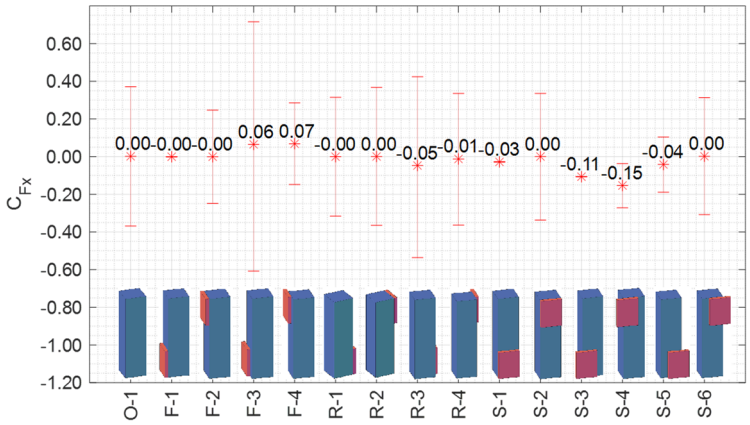

Fig. 11. Wind force coefficient in x-direction (C_{Fx})

O-1, leading to the minimal variations in C_{Fy}.

Regarding the placement of the overhangs at the lower and upper part of the building on the same face, two distinct subgroups can be identified: the first consists of overhangs that are aligned with the building width (F-1 to F-2 and R-1 to R-2), while the second subgroup involves overhangs located in a staggered configuration (F-3 to F-4 and R-3 to R-4). The former subgroup shows the absolute value of C_{Fy} is smaller in lower overhang configurations compared to upper configurations. Whereas the latter group presents the opposite trend with the former subgroup. In the first subgroup, the decrease in the absolute value of C_{Fy} in cases F-1 and R-1 compared to F-2 and R-2 respectively is attributed to the decrease in pressure at the top of the rear surface compared to O-1. On the other hand, considering the second subgroup, taking R-3 and R-4 as an example (shown in **Fig. 10**), the increase in the absolute value of C_{Fy} in the lower overhang configuration (R-3) compared to the upper overhang configuration (R-4) is due to the decrease in the negative pressure on the rear face and increase in the positive pressure on the upwind face of the overhang. **Fig. 10** shows that the C_{Fy} is not noticeably affected by the pressures on the front faces of the main building in these configurations, the opposite trend in the two subgroups could be explained by the aforementioned shift in the location of the rear stagnation point and the stagnation point on the upwind face of the staggered overhang.

4.2 EFFECT OF OVERHANG ON ACROSS-WIND FORCE

Fig. 11 presents the force coefficient and its fluctuation in the crosswind direction (C_{Fx}) for both the square building and 14 buildings with attached overhang. The fluctuation range of C_{Fx} is more significant compared to the along-wind force coefficients. The flow patterns of wind in the across-wind direction are characterized by increased complexity and turbulence in comparison to the relatively smoother flow observed in the along-wind direction. This turbulence is caused by the interaction of the wind with the building's edge and surface roughness. A strong shear layer is formed between the building edge and the reattachment point which is located on the side face in the case of a square section. Within this shear layer, vortices persistently exist, contributing to the fluctuations experienced in the across-wind direction.

The mean C_{Fx} is distributed approximately around zero. The greatest absolute values of mean C_{Fx} are observed in the staggered configuration of overhang on the upwind side face S-3 and S4 with values -0.11 to -0.15 respectively. These cases exhibit substantial deviations from O-1 in the wind pressure coefficient distributions on the side surfaces presented in **Fig. 12**. S-3 demonstrates positive pressure on the overhang on the building side and negative pressure on the opposite side. The proximity of the overhang to the windward wall of the building induces a positive pressure due to the stagnation point of the incoming flow being situated on the overhang. Conversely, the opposite side experiences a localized and intense negative pressure resulting from the conical vortex created by the detached wind flow at the upper section of the overhang. S-4 generates positive pressure on the overhang on the building side and negative pressure on the opposite side, the same as S-3. However, the negative pressure area on the opposing side of the building is more extensive in S-4 compared to S-3, and the negative pressure is heightened due to wind separation occurring at both the top and bottom of the overhang. On the other hand, in the case of

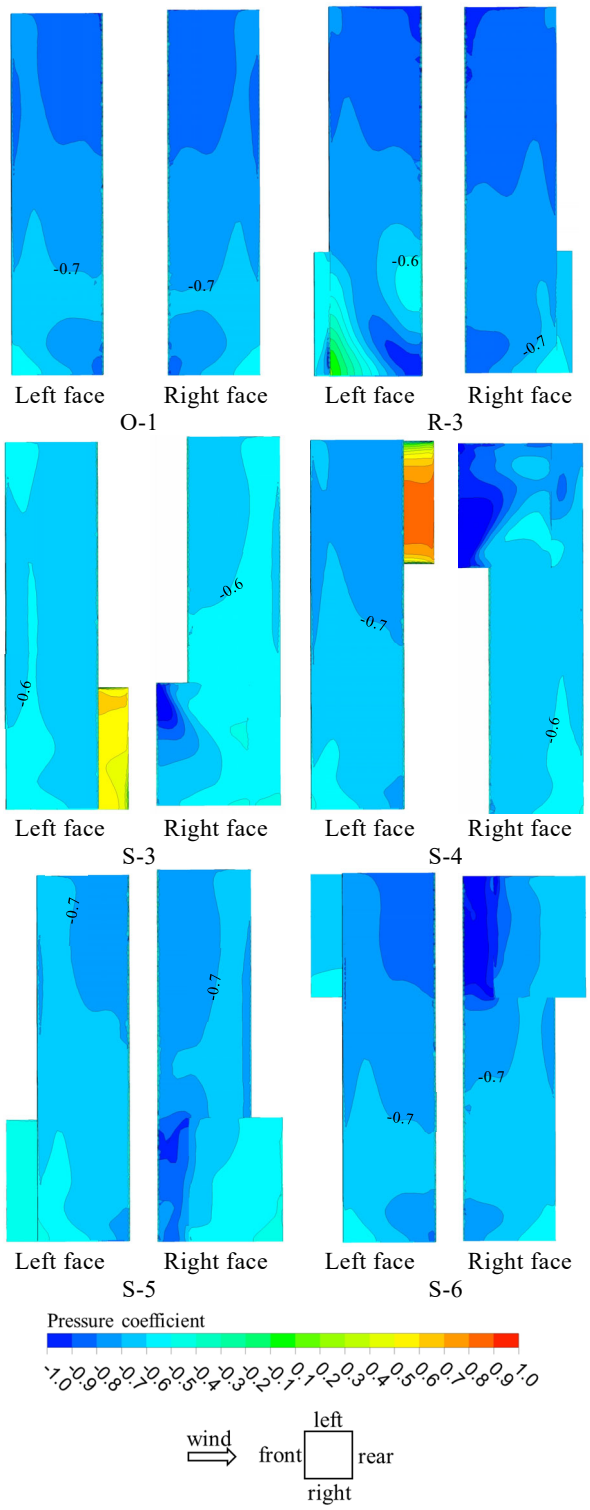

Fig. 12. Mean pressure coefficient distribution on the left and right faces.

S-5 and S-6, where the overhang is located on the downwind side, a pronounced negative pressure region is observed on the overhang wall at the upwind corner, whereas no positive pressure region is present on either side. The flow separation point may be located on the building edge, and the vortices are formed in the space between the building and the overhang. These vortices cause a significantly high negative pressure in that region. Consequently, in contrast to the S-3 and S-4 models, the decrease in the C_{Fx} in the S-5 and S-6 models, when compared to the O-1 model, does not exhibit a significant difference.

5. CONCLUSION

The wind characteristics of a high-rise building with rectangular overhangs at various locations are examined through numerical analysis. The main conclusions of this study are as follows.

- The attachment of overhangs has a noticeable effect on the along-wind force coefficient. Locating the overhang at the lower front on the main building, the along-wind force coefficient differs by -10% to 20% compared to principal building. On the other hand, the difference is small in upper front and rear configuration. The reason could be attributed to the change in the rear stagnation point.
- In the case of the front and rear overhangs, the opposite trend in along-wind force coefficient for upper and lower overhang buildings is observed between the staggered configuration and fixed configuration.
- When the overhang is arranged in a staggered configuration on the windward side, the local wind pressure distribution around the overhang causes higher mean across-wind force mainly due to the stagnation point of the incoming flow.

These conclusions are limited to CFD simulation. Further studies using wind tunnel experiments will be conducted in the future.

References

1) Sumitomo Mitsui Construction : "Sulatto V Tower", 2020, URL: https://www.smcon.co.jp/service/sukkit/sulatto-v-tower/
2) Yoshida Akihito, Masuyama Yuka, and Katsumura Akira : "Characteristics of Negative Peak Wind Pressure acting on Tall Buildings with Step on Wall Surface", International Journal of High-Rise Buildings, Vol.8, No.4, pp.283-290, 2019
3) Isaev SA and Lysenko DA : "Calculation of unsteady flow past a cube on the wall of a narrow channel using URANS and the Spalart–Allmaras turbulence model", Journal of

Engineering Physics and Thermophysics, Vol.82, No.3, pp.488-495, 2009

4) Tominaag Yoshihide : "Flow around a high-rise building using steady and unsteady RANS CFD: Effect of large-scale fluctuations on the velocity statistics", Journal of Wind Engineering and Industrial Aerodynamics, Vol.142, pp.93-103, 2015

5) Rajasekarababu KB, Vinayagamurthy G, and Selvi Rajan S : "Evaluation of CFD URANS Turbulence Models for the Building under Environmental Wind Flow with Experimental Validation", Journal of Applied Fluid Mechanics, Vol.15, No.5, pp.1387-1401, 2022

6) Versteeg Henk Kaarle and Malalasekera Weeratunge : "An introduction to computational fluid dynamics: the finite volume method", Pearson Education, 2007

7) Laneville A, Gartshore Is, and Parkinson Gv : "An explanation of some effects of turbulence on bluff bodies", Proceeding 4th International Conference Wind Effects on Buildings and Structures, Heathrow, Cambridge University Press, 1977